INVESTIGATION OF FLOW PHENOMENA IN CURVED CHANNELS OF RECTANGULAR CROSS-SECTION

Milan Sedlář*, Jaromír Příhoda**

The aim of this work was to model numerically the flow phenomena occurring in turbulent flows through curved diffusers of the rectangular cross-section. All investigated diffusers have the cylindrical inner wall, the area ratio 1.5 and the flow turn angle 90°. They differ in the ratio of the inner wall radius and the diffuser height. Calculations were carried out for various inlet velocities resulting in the Reynolds numbers approximately in the range of 1×10^5–1×10^6. The ANSYS CFX package was used, employing both the k-ω/k-ε SST turbulence model by Menter and the RSM model by Launder, Reece and Rodi. Structured mono-block grids refined in the regions with high velocity gradients were used, representing a numbers of nodes from 1.4 mil. to 1.8 mil. grid points.

Key words: *turbulent flow in curved diffuser, CFD analysis, 3D separation, secondary flows, skin-friction lines*

1. Introduction

The viscous flow in curved channels and diffusers is a very important topic of many numerical and experimental studies. These hydraulic shapes are widely used in turbomachinery, aircraft applications, HVAC and other systems. A lot of publications deal with the pressure distribution, velocity profiles and separation regions inside such channels and with the corresponding energy losses. In this field the article follows the theoretical and experimental work presented by Příhoda and Sedlář [2] and Příhoda et al. [3]. Nevertheless, the aim of this work was to model numerically the flow phenomena occurring in the turbulent flow through the curved diffusers of the rectangular cross-section, as well as to find a relationship between the hydraulic losses, flow patterns and dimensionless parameters describing the geometry and flow quantities. Two main phenomena are of fundamental interest: the separation on the inner wall and the secondary flows, normal to the main flow direction.

The three-dimensional separation is a very difficult subject to be described, see e.g. Shimizu et al. [4], Tobak and Peake [5], and Winters [6]. At present our understanding of the three-dimensional separations is based both on the experimental observations using special flow visualization techniques and the CFD analysis. Between the experimental methods, especially the oil-film technique plays the leading role. It enables to visualise the patterns of the skin-friction lines on the surfaces of the channel. Many authors tried to define 3D separation on the basis of the skin-friction lines, forming the convergence of skin-friction lines onto a particular skin friction line as the necessary condition for a separation. Here the pres-

* RNDr. M. Sedlář, CSc., SIGMA Research and Development Institute, Jana Sigmunda 79, Lutín, CR
** prof. Ing. J. Příhoda, CSc., Institute of Thermomechanics, ASCR, v.v.i., Dolejškova 5, Praha, CR

ence of the saddle point plays a very important role. We will adopt the terminology used by Tobak and Peake [5]. Here the skin-friction line emerging from a saddle point (Fig. 1) is the global line of separation and leads to the global flow separation. In the contrary case, the skin-friction line on which other lines converge does not originate from the saddle point; this is the local line of separation, leading to the local flow separation. The definition of the saddle point (and the other critical ones) is based on the eigenvalues of the velocity gradient matrix and can be found e.g. in the work of Tobak and Peake [5].

There are two types of secondary flows in curved channels. The first one is formed by the centrifugal forces acting on the fluid in the bend and resulting in one or more pairs of counter-rotating vortices. The second one can be found in non-circular channels, both curved and straight, near the corners (see Hur et al. [1]) and it is associated with turbulence. The turbulence-driven secondary flows result from the normal Reynolds stresses and can be predicted only with the turbulence models which simulate anisotropic features of turbulence, in particular the differences between the various Reynolds stresses. In curved channels, the turbulence-driven secondary flows are usually much less intensive comparing to the secondary flows of the first type. In our study, we concentrate on the first type secondary flows only.

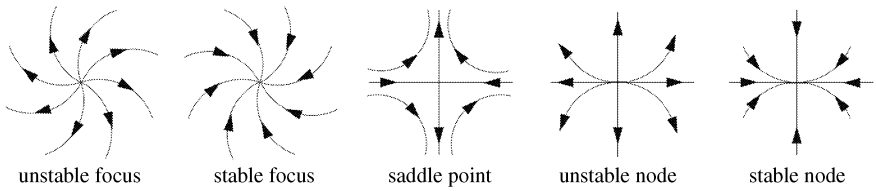

Fig.1: Critical points in flow patterns

An important parameter, which describes the structure of the secondary flows in curved ducts, is the Dean number De defined as follows

$$De = \frac{Re}{\sqrt{\frac{R}{D_\mathrm{h}}}} \,, \tag{1}$$

where Re is the Reynolds number, R is the radius of curvature and D_h is the hydraulic diameter. The Dean numbers corresponding with the flows examined in this study range from $4{\times}10^4$ to $1{\times}10^6$. Unfortunately most studies concerning relations between the Dean number and the structure of secondary flows are published for low Dean number values (1–900) and there is a lack of information concerning flows for Dean numbers higher then 1000. Another problem arises from the fact that the results obtained in curved channels are difficult to generalize for flows in diffusers where the hydraulic diameter changes and the 3D separation on the inner wall highly influences the secondary flow structure.

Although computational methods are not still completely satisfactory in view of quantitative prediction of flow losses and complex flow phenomena, the CFD tools are very useful in analysing flow fields as they give a very detailed picture of flow inside the investigated domains. In a very large number of points the flow and turbulence quantities are calculated and can be interpreted both in the graphical and the numerical way. In our study the loss coefficient will be the most important integral quantity. Concerning the topology of three-dimensional separated flows, the surface skin-friction lines will be very useful as they

simulate the multi-colour oil-film flow visualization technique. To describe the secondary flows inside the channels, secondary flow streamlines will be used as well.

2. Diffuser geometry

All investigated diffusers are the plane ones, which means that they have the constant height $B = 0.2\,\mathrm{m}$. The diffusers have the cylindrical inner wall with the wall radius R_i, the area ratio $AR = W_2/W_1 = 1.5$ and the flow turn angle 90°, as it is seen in Fig. 2. They differ in the ratio R_i/W_1 which changes from 1 to 6. In all cases the computational domain consists of the straight inlet part of the square cross-section $W_1 \times B = 0.2 \times 0.2\,\mathrm{m}$ and the length equal to $L_1 = 15\,W_1$, the diffuser and the straight outlet part of the rectangular cross-section $W_2 \times B = 0.3 \times 0.2\,\mathrm{m}$ and the length equal to $L_2 = 23\,W_1$ (see Příhoda et al. [3]).

3. Numerical simulation

The ANSYS CFX package was used to solve the three-dimensional Reynolds-averaged Navier-Stokes equations together with the turbulence model. Both the k-ω/k-ε SST turbulence model by Menter and the RSM model by Lauder, Reece and Rodi were used during the calculations. Because of better description of the near-wall flow by the SST model, all results presented in this study are based on this turbulence model. Structured mono-block grids refined in the regions with high velocity gradients were used, representing numbers of nodes from 1.4 mil. to 1.8 mil. grid points.

In the calculations the whole channel was modelled, that means no symmetry plane was used to prevent the analysis from an artificial symmetry of the solution. At the inlet, the uniform normal velocity was prescribed, with values $U_\mathrm{m} = 0.5; 1; 1.5; 2; 3; 4$ and $6\,\mathrm{m/s}$, which represent the Reynolds numbers $Re = U_\mathrm{m} W_1/\nu$ from 97000 to 1164000. Constant values of the turbulence level $Tu = 0.04$ and turbulent length scale $L_\mathrm{t} = 0.005\,\mathrm{m}$ have been applied at the inlet, according to the experimental data obtained by Příhoda et al. [3]. At the outlet the average static pressure was set. The water at the temperature 20 °C was employed as the working fluid.

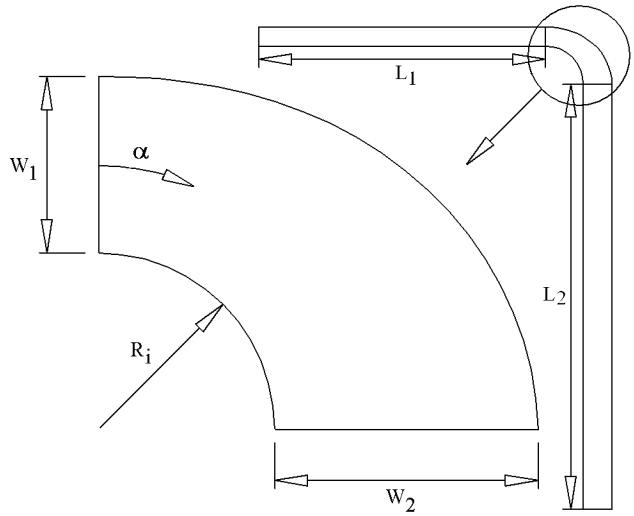

α [°]	Width [mm]
0	200
5	201,1
10	203,5
15	207,2
20	212,2
25	218,1
30	224,8
35	232,2
40	239,9
45	247,9
50	256
55	263,9
60	271,4
65	278,5
70	284,9
75	290,3
80	294,8
85	298
90	300

Fig.2: Diffuser geometry

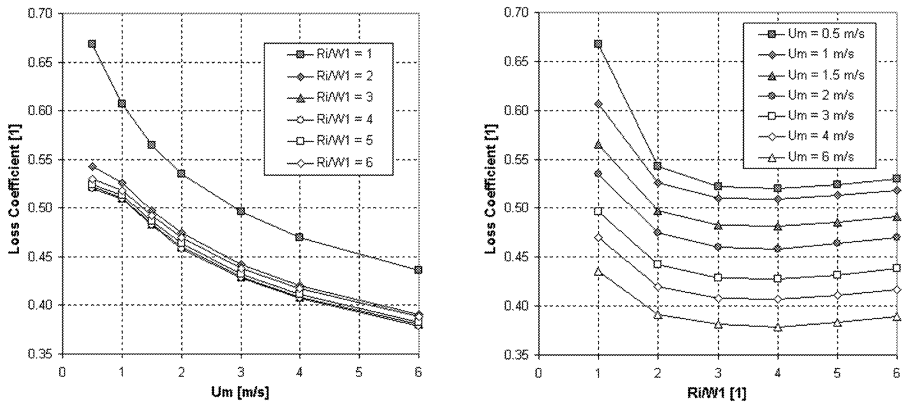

Fig.3: Loss coefficient as a function of inlet velocity U_m and ratio R_i/W_1

Figure 3 shows the calculated loss coefficient as a function of the ratio R_i/W_1 and the inlet velocity U_m. Here the loss coefficient is defined as follows

$$\zeta_\mathrm{d} = \frac{p_{\mathrm{c}1} - p_{\mathrm{c}2}}{\frac{\varrho\, U_\mathrm{m}^2}{2}} \ , \tag{2}$$

where $(p_{\mathrm{c}1} - p_{\mathrm{c}2})$ is the total pressure loss due to the flow through the diffuser and $\varrho\, U_\mathrm{m}^2/2$ is the mean dynamic pressure at the diffuser inlet. It can be seen that the minimum loss coefficients lies somewhere close to the ratio $R_\mathrm{i}/W_1 = 4$. For higher values of R_i/W_1, the pressure losses caused by the separation and secondary flows decrease very slowly and increasing wall friction losses (the wet surface area increases with R_i/W_1) dominate.

4. Separation patterns

In the presented range of computations four basic patterns of the skin-friction lines on the diffuser inner wall can be found: the three ones for a global separation and one pattern for a local separation. All the three global separations are the separations, which correspond to the classical idea of the separation; here the flow separates from the wall and forms a region in which the fluid flows upstream (opposite the mean flow). As far as the local flow separation is concerned, here the fluid separates from the wall but no region of the backflow can be found.

4.1. Massive global separation (separation type A)

In the case of the massive global separation, the main separation region starts with two saddle points separated by a focus. That is why this separation is (the only one) asymmetric in its nature. The global line of separation is joined with foci on both sides, forming horn-type dividing surfaces. Downstream the pair of foci one nodal point of attachment and three limiting skin friction lines can be found close to the mean-line of the inner wall. On each side of the inner wall close to the rectangular corner there are limiting two skin friction lines accompanied by a small global separation. Unfortunately the global separations in the corners are so narrow that it is not possible to check the topology of these separations in detail. A typical case of separation type A can be found in the diffuser with ratio $R_\mathrm{i}/W_1 = 1$ and $U_\mathrm{m} = 0.5\,\mathrm{m/s}$ ($Re = 97000$).

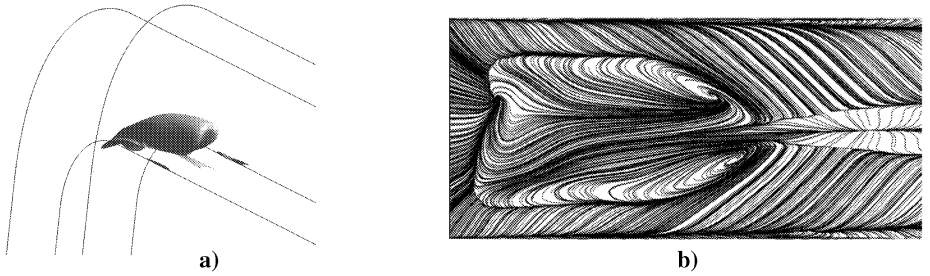

Fig.4: Global separation on inner wall of diffuser with ratio $R_i/W_1 = 1$ and $U_m = 0.5\,m/s$ ($Re = 97000$); a) 3D view; b) skin-friction lines on inner wall

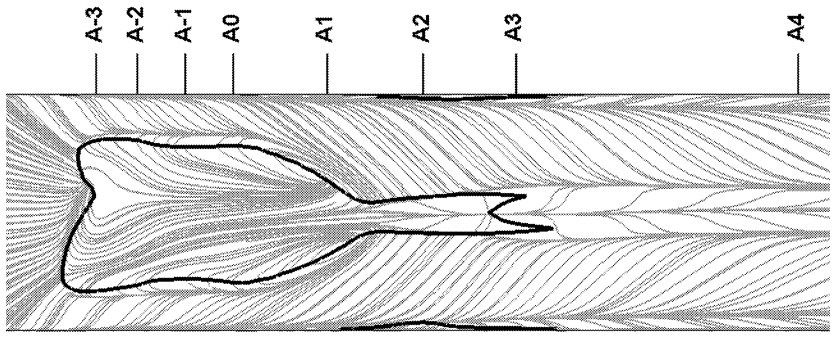

Fig.5: Backflow region for diffuser with ratio $R_i/W_1 = 1$ and $U_m = 0.5\,m/s$ ($Re = 97000$); projection on inner wall (dark line) and location of cross-sections A-3 – A4

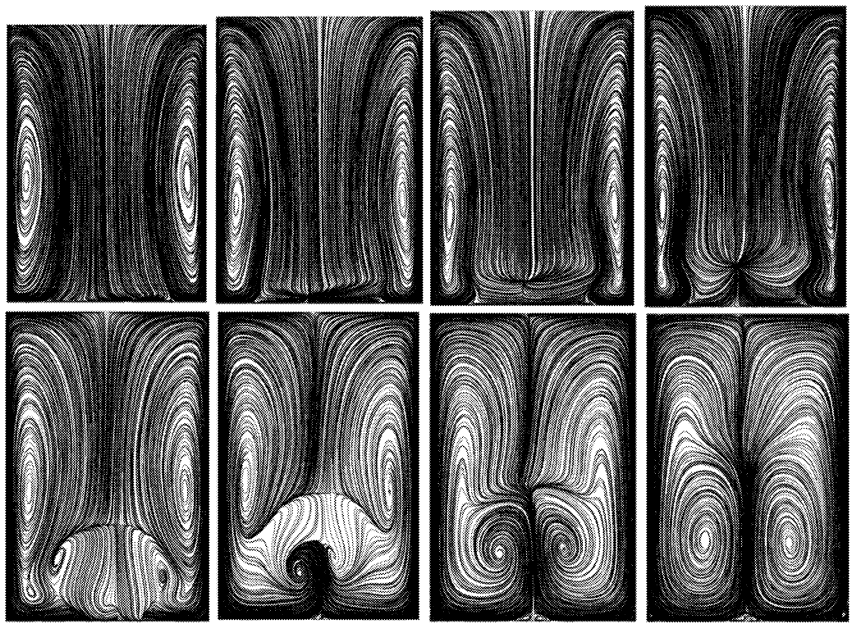

Fig.6: Cross-flow streamlines in cross-sections A-3, A-2, A-1, A0, A1, A2, A3, A4 for diffuser with ratio $R_i/W_1 = 1$ and $U_m = 0.5\,m/s$ ($Re = 97000$)

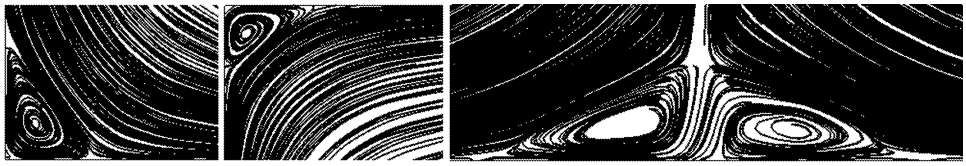

Fig.7: Details of bottom-left and top-left corners and bottom-central part of cross-section A3 for diffuser with ratio $R_i/W_1 = 1$ and $U_m = 0.5\,m/s$ ($Re = 97000$)

Figure 4 shows the size and shape of the backflow region and the skin-friction lines on the inner wall. Figure 5 presents a boundary of the backflow region on the inner wall. Figure 6 shows cross-flow streamlines in cross-sections A-3, A-2, A-1, A0, A1, A2, A3 and A4. The basic cross-section A0 is located in the position, where the diffuser turns into the straight outlet part ($\alpha = 90°$). A-3 to A-1 are the cross-sections of the diffuser at $\alpha = 54°$, $66°$ and $78°$. A1 to A4 are the cross-sections of the straight outlet part located 80, 160, 240 and 480 mm downstream A0. The secondary flow in the diffuser is very complex. Besides the vortices visible in Fig. 6, there are other vortices which can be seen only in a zoom, e.g. vortices in the corners or a pair of small vortices at the bottom, between the two primary ones (Fig. 7).

4.2. Typical case of global separation (separation type B)

In this case one saddle point in combination with a nodal point of attachment can be found on the mean-line of the inner wall, forming a global separation. The global line of separation is joined with foci on both sides, forming horn-type dividing surfaces. On both sides of the inner wall close to the rectangular corners there are limiting skin friction lines accompanied by small global separations (similar to the case of separation type A). A typical case of separation type B can be found in the diffuser with ratio $R_i/W_1 = 1$ and $U_m = 2\,m/s$ ($Re = 388000$).

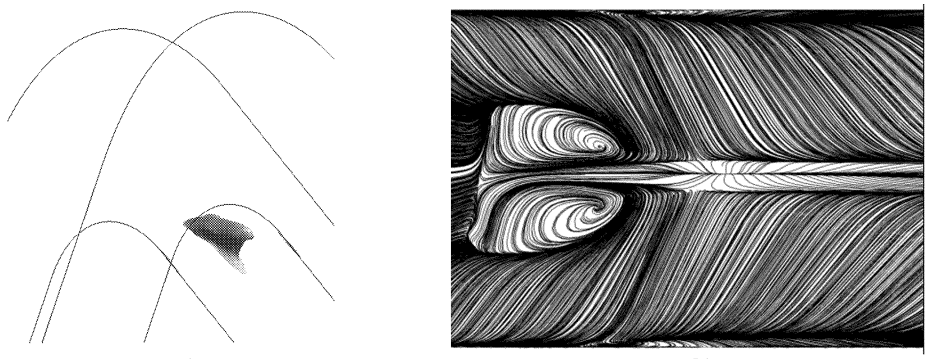

a) **b)**

Fig.8: Global separation on inner wall of diffuser with ratio $R_i/W_1 = 1$ and $U_m = 2\,m/s$ ($Re = 388000$); a) 3D view; b) skin-friction lines on inner wall

Figure 8 shows the size and shape of the backflow region and skin-friction lines on the inner wall. Figure 9 presents a boundary of the backflow region on the inner wall. Figure 10 shows the cross-flow streamlines in the cross-sections B-3, B-2, B-1, B0, B1, B2, B3 and B4. The basic cross-section B0 is located in the position, where the diffuser itself borders

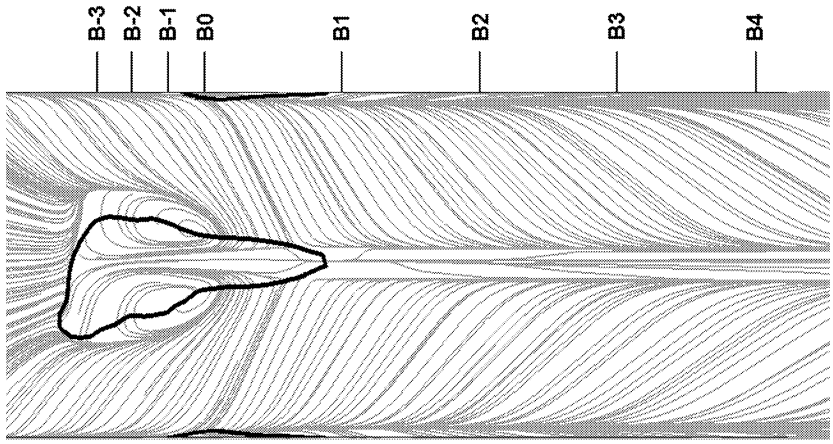

Fig.9: Backflow region for diffuser with ratio $R_\mathrm{i}/W_1 = 1$ and $U_\mathrm{m} = 2\,\mathrm{m/s}$ ($Re = 388000$); projection on inner wall (dark line) and location of cross-sections B-3 – B4

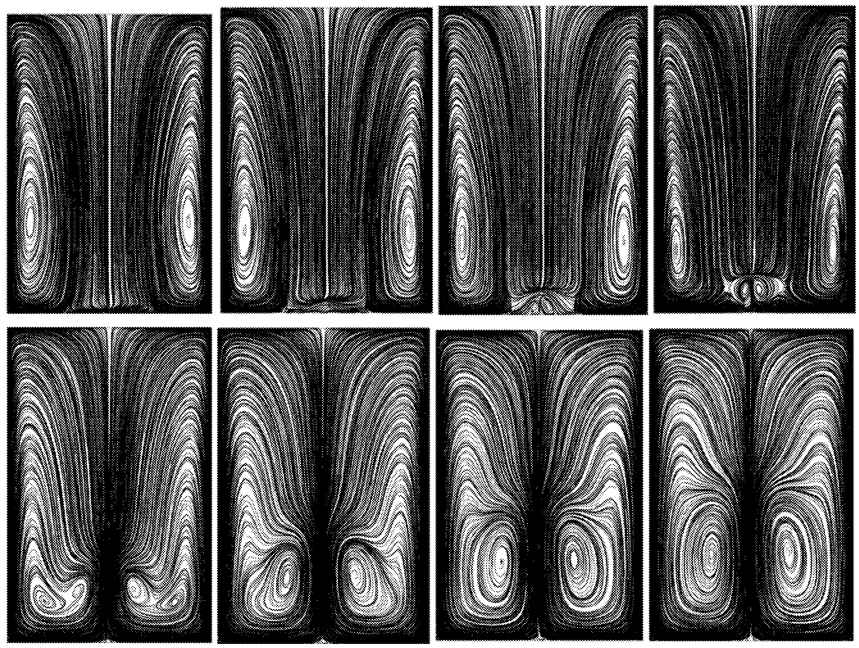

Fig.10: Cross-flow streamlines in cross-sections B-3, B-2, B-1, B0, B1, B2, B3, B4 for diffuser with ratio $R_\mathrm{i}/W_1 = 1$ and $U_\mathrm{m} = 2\,\mathrm{m/s}$ ($Re = 388000$)

with the straight outlet part ($\alpha = 90°$). B-3 to B-1 are the cross-sections of the diffuser at $\alpha = 72°$, $78°$ and $84°$. B1 to B4 are the cross-sections of the straight outlet part located 80, 160, 240 and 320 mm downstream B0.

4.3. Simple case of global separation (separation type C)

In the case of the separation type C one saddle point in combination with a nodal point of attachment can be found on the mean-line of the inner wall, forming a global separation. On

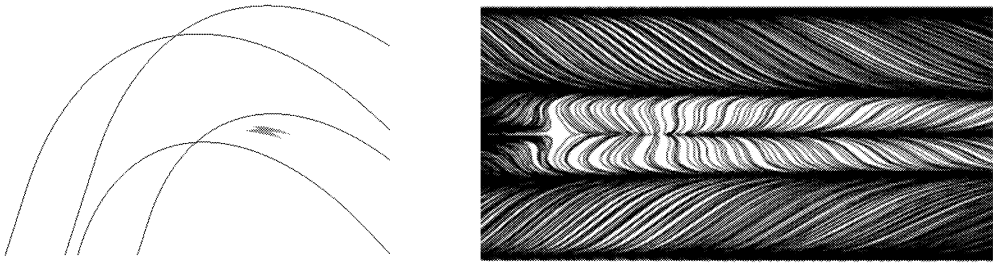

a) b)

Fig.11: Global separation on inner wall of diffuser with ratio $R_i/W_1 = 4$ and $U_m = 0.5\,m/s$ ($Re = 97000$); a) 3D view of backflow region; b) skin-friction lines on inner wall

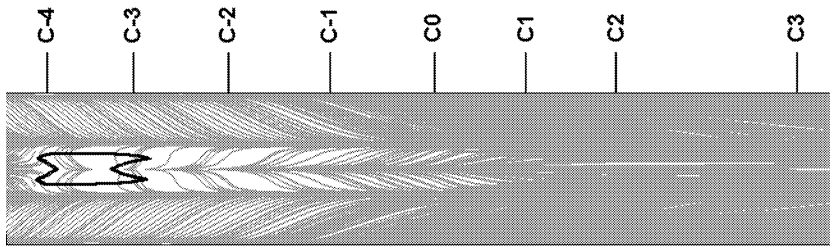

Fig.12: Backflow region for diffuser with ratio $R_i/W_1 = 4$ and $U_m = 0.5\,m/s$ ($Re = 97000$); projection on inner wall (dark line) and location of cross-sections C-4 – C3

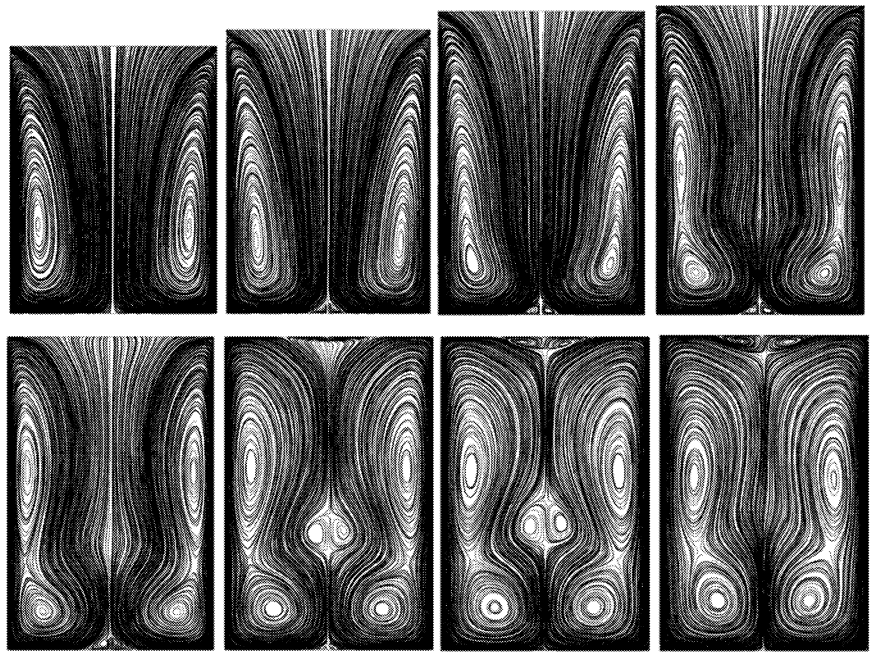

Fig.13: Cross-flow streamlines in cross-sections C-4, C-3, C-2, C-1, C0, C1, C2, C3 for diffuser with ratio $R_i/W_1 = 4$ and $U_m = 0.5\,m/s$ ($Re = 97000$)

each side of the inner wall close to the rectangular corner there is a limiting skin friction line accompanied by a local separation. No foci can be found in this global separation pattern. A typical case of separation type C can be found in the diffuser with ratio $R_i/W_1 = 4$ and $U_m = 0.5\,m/s$ ($Re = 97000$).

Figure 11 shows the size and shape of the backflow region and the skin-friction lines on the inner wall. Figure 12 presents the boundary of the backflow region on the inner wall. Figure 13 shows the cross-flow streamlines in cross-sections C-4, C-3, C-2, C-1, C0, C1, C2 and C3. The basic cross-section C0 is located in the position $\alpha = 90°$. C-4 to C-1 are the cross-sections of the diffuser at $\alpha = 50°$, $60°$, $70°$ and $80°$. C1 to C3 are the cross-sections of the straight outlet part located 120, 240 and 480 mm downstream C0.

4.4. Case of local separation (separation type D)

No saddle point and no nodal point of attachment can be found on the mean-line of the inner wall in the case of the local separation. In this type of separation the skin-friction lines simply diverge and then converge, forming an 'island' boarded by two limiting skin-friction lines (Fig. 14). Another limiting skin-friction line can be found in the mean-line of the inner wall. No separation on both sides of the inner wall close to the rectangular corners can bee seen as well as no backflow region inside the diffuser. A typical case of separation type D can be found in the diffuser with ratio $R_i/W_1 = 4$ and $U_m = 2\,m/s$ ($Re = 388000$).

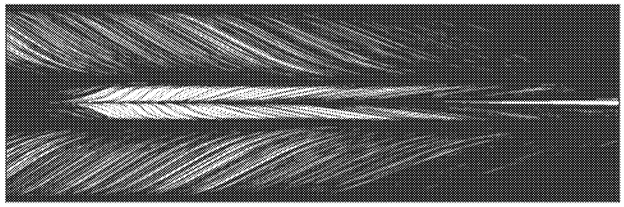

Fig.14: Global separation on inner wall of diffuser with ratio $R_i/W_1 = 4$ and $U_m = 2\,m/s$ ($Re = 388000$)

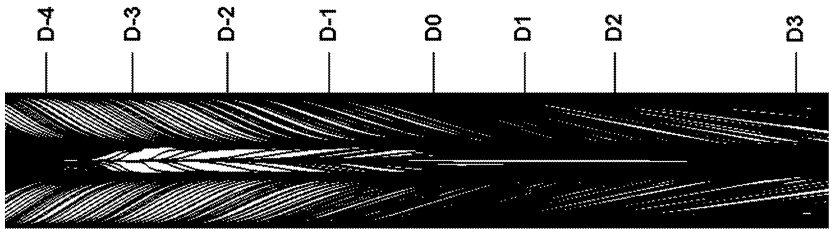

Fig.15: Location of cross-sections D-4 – D3 for diffuser with ratio $R_i/W_1 = 4$ and $U_m = 2\,m/s$ ($Re = 388000$)

Figure 15 presents the location of the cross-sections D-4 – D3, in which the cross-flow streamlines are examined (Fig. 16). The basic cross-section D0 is located in the position $\alpha = 90°$. D-4 to D-1 are the cross-sections of the diffuser at $\alpha = 50°$, $60°$, $70°$ and $80°$. D1 to D3 are the cross-sections of the straight outlet part located 120, 240 and 480 mm downstream D0.

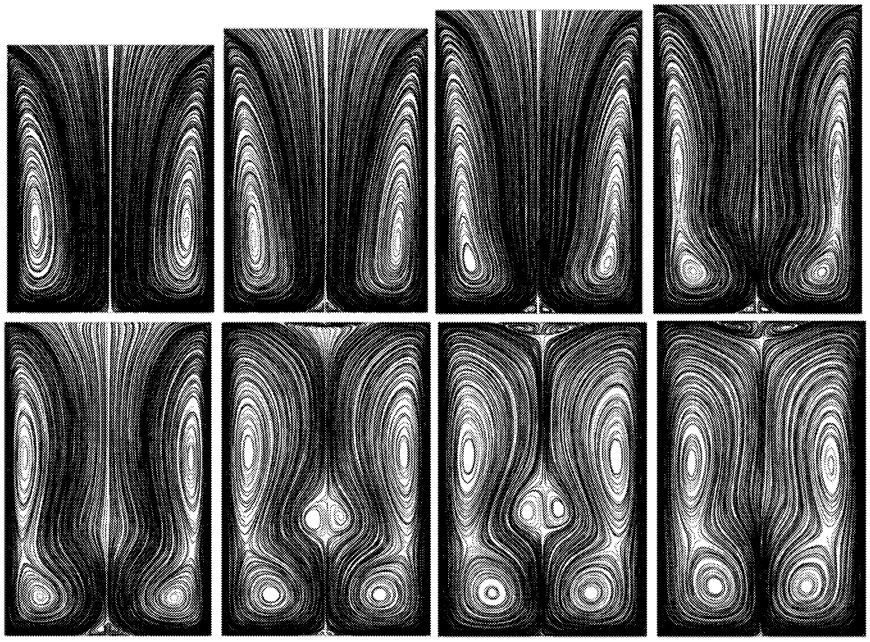

Fig.16: Cross-flow streamlines in cross-sections D-4, D-3, D-2, D-1, D0, D1, D2, D3 for diffuser with ratio $R_i/W_1 = 4$ and $U_m = 0.5\,m/s$ ($Re = 388000$)

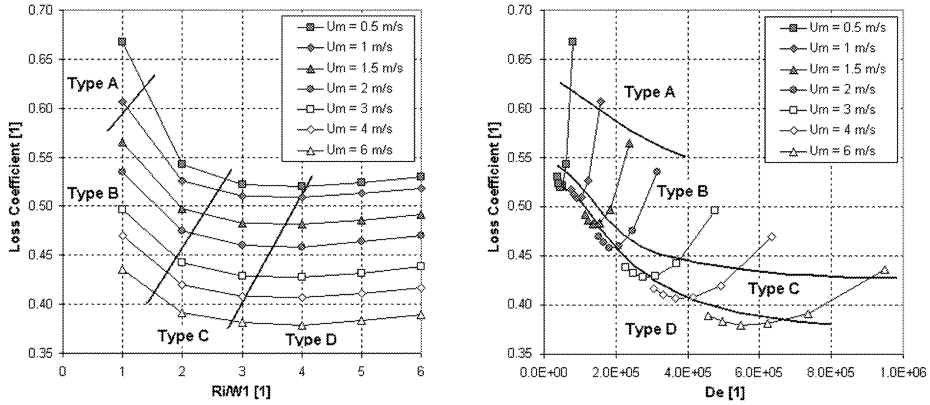

Fig.17: Separation types for different diffuser geometries and different Dean numbers

5. Conclusions

Figure 17 shows the calculated loss coefficient as the functions of the ratio R_i/W_1 and the Dean number. Regions of different separation types are marked in both graphs. In the presented results it can be seen that the separated flow in curved diffusers of the rectangular cross-section is very complex and depends both on the diffuser geometry and the Reynolds number. The ratio R_i/W_1 seems to be the most important parameter, which determines the type of the separation. The Dean number has only small influence on the separation type. To be able to sort the separation type on the basis of only one dimensionless parameter, the

combinations of both the ratio R_i/W_1 and the Reynolds number in the form

$$C = \left(\frac{R_\mathrm{i}}{W_1}\right)^a Re^b \tag{3}$$

were tested statistically. The combination with the exponents $a = 1$ and $b = 0.2$ gives the best results as all the regions of different separation types can be separated by the lines representing the constant values of the dimensionless parameter C (Fig. 18).

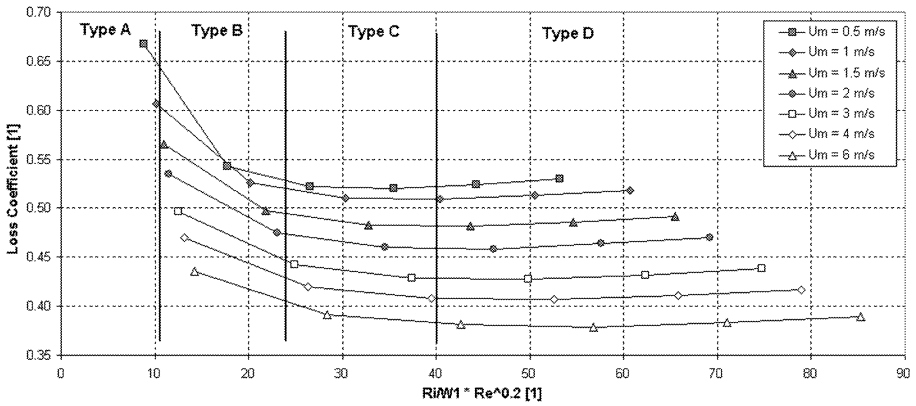

Fig.18: Separation types as function of dimensionless parameter C

As far as the secondary flows are concerned, they are influenced first of all by the separation, forming different structures of multiple vortices, which are very complex especially in the regions where the horn-type dividing surfaces appear in the case of the separations type A and B.

Acknowledgement

The work was supported by the research project No. 101/07/1508 funded by the Czech Science Foundation and by the Research Plan No. AV0Z20760514.

References

[1] Hur N., Thangam S., Speziale C.G.: Numerical study of turbulent secondary flows in curved ducts, Trans. ASME, J. Fluids Eng., Vol. 112, 205–211, 1990
[2] Příhoda J., Sedlář M.: Analysis of turbulent flow in curved channels and diffusers, Proc. 4th Water Management Conference 2004, ECON Publ. Brno, 383–390, 2004 (in Czech)
[3] Příhoda J., Šulc J., Sedlář M., Zubík P.: Numerical and experimental modelling of turbulent flow in curved channels and diffusers, Eng. Mechanics, Vol. 12, 429–440, 2005
[4] Shimizu Y., Futaki Y., Martin C.S.: Secondary flow and hydraulic losses within sinuous conduits of rectangular cross section, Trans. ASME, J. Fluids Eng., Vol. 114, 583–600, 1992
[5] Tobak M., Peake D.J.: Topology of three-dimensional separated flows, Ann. Rev. Fluid Mech., Vol. 14, 61–85, 1982
[6] Winters K.H.: A bifurcation study of laminar flow in a curved tube of rectangular cross-section, J. Fluid Mechanics., Vol. 180, 343–369, 1987

Received in editor's office: April 6, 2007
Approved for publishing: June 1, 2007